# Controlling quantum many-body systems using reduced-order modeling

I. A. Luchnikov,* M. A. Gavreev,† and A. K. Fedorov‡
*Russian Quantum Center, Skolkovo, Moscow 143025, Russia*
*and National University of Science and Technology (MISIS), Moscow 119049, Russia*

(Received 14 September 2023; revised 2 December 2023; accepted 6 December 2023; published 13 February 2024)

Quantum many-body control is among the most challenging problems in quantum science due to its outstanding computational complexity in a general case. We propose an efficient approach to a class of many-body quantum control problems, where time-dependent controls are applied to a sufficiently small subsystem. The method employs a tensor-network scheme to construct a reduced-order model of a subsystem's non-Markovian dynamics. The resulting reduced-order model serves as a digital twin of the original subsystem. Such twins allow significantly more efficient dynamics simulation, which enables the use of a gradient-based optimization toolbox in the control parameter space. This approach to building control protocols takes advantage of non-Markovian dynamics of subsystems by design. We validate the proposed method by solving control problems for quantum spin chains. In particular, the approach automatically identifies control sequences for exciting and guiding quasiparticles to recover and transmit quantum information across the system. In addition, we find generalized spin-echo sequences for a system in a many-body localized phase enabling significant revivals. We expect our approach can be useful for ongoing experiments with noisy intermediate-scale quantum devices.

DOI: 10.1103/PhysRevResearch.6.013161

## I. INTRODUCTION

Recent progress in the field of quantum technologies has raised many challenging engineering, mathematical, and computational problems. Among those problems is the problem of quantum optimal control. Despite tremendous progress in this field [1–8], quantum optimal control methods are extremely challenging to scale to many-body systems. The crucial challenge is that the underlying quantum many-body dynamics simulation problem requires resources, which grow exponentially with the number of degrees of freedom in the general case. Optimization methods used to adjust a control signal require repeating this simulation many times, making the problem even harder.

Despite the difficulty of the quantum many-body control problems, in general, there are several instances where this problem can be resolved at least partly. For example, gradient-free optimization methods combined with tensor-networks-based dynamics simulation were applied to many-body ground state preparation [9–12]. Recently, methods using reinforcement learning techniques have been proposed [13,14]; such approaches can also be viewed as gradient-free optimization since they do not use the gradient of the reward function. The gradient-free optimization-based control methods, however, are generally expected to be less efficient than gradient-based methods [15]. Recently, Ref. [16] demonstrated the advantage of gradient-based methods for the problem of ground-state preparation by crossing the superfluid to Mott-insulator phase transition in the Bose-Hubbard model.

Here we propose a different approach to a class of problems where a sufficiently small (target) subsystem of a many-body system is subject to time-dependent control. We start by building a *reduced-order* [17–20] model (ROM) that describes the dynamics of a subsystem as accurately as the complete model, but contains no information that is irrelevant to the subsystem dynamics. This is on par with the information bottleneck method [21,22] when one tries to build a predictive model of some phenomenon based on a minimal number of parameters. Such a reduction effectively keeps track of the relevant degrees of freedom in the environment, discarding those that have little or no effect on the dynamics of the target subsystem.

Reduced order modeling allows one to reduce the dimension of the Hilbert space to the effective one, which can be orders of magnitude smaller than in the original problem. This opens the possibility to engage a powerful toolbox of gradient-based optimization methods and make, in particular, the calculation of the gradient of the loss function using automatic differentiation techniques [23] usable.

To build a ROM, we employ tensor-network techniques that are widely used for dimensionality reduction in quantum many-body physics [24,25] and applied mathematics [26,27]. Combining the developed order reduction scheme with gradient-based optimization yields an efficient yet simple method for quantum many-body control.

*luchnikovilya@gmail.com
†m.gavreev@rqc.ru
‡akf@rqc.ru

We use our approach to automatically design protocols for manipulating information propagation in strongly interacting systems. First, we consider a 1D XYZ quantum Heisenberg chain with extra fields that break integrability. For simplicity, we choose a single spin as the subsystem where time-dependent controls are applied. Our algorithm is able to find sequences that restore quantum information locally or transmit it to another end of the chain. Physically, the identified sequences of local operations inject and reabsorb long-lived quasiparticles optimally. Further, we apply the optimization method to the many-body localized (MBL) phase. We can find control protocols for local dynamics inversion that outperform existing spin-echo-type protocols for MBL systems [28]. Thus, our approach enables the automated discovery of optimal generalized spin-echo sequences in interacting systems.

The method described here can be readily applied in experiments with the current generation of noisy intermediate-scale quantum devices [29–31]. Various quantum computing platforms, including programmable Rydberg simulators, trapped ions, isolated spin impurities in solids, and superconducting circuits arrays realize 1D spin chains [32–39] with the possibility to control qubits individually by means of optical or microwave pulses. Our approach shows that the non-Markovianity of a many-body environment can generate excitations and information spreading across the system. We expect that a modification of our approach may also be used for many-body state preparation, environment cooling, etc.

Here we are focused on the the realization of the control method in the coherent phase of quantum many-body systems assuming specific techniques to avoid fast thermalization. In the thermalized phase, one can use an influence matrix approach [40–42] that is a similar technique aimed at thermal environments compression in the thermodynamic limit.

Our paper is organized as follows. In Sec. II, we describe our general approach to ROM building. We illustrate this approach with the example of a quantum spin chain, our primary quantum many-body model of interest, in Sec. III A. In Sec. III B, we discuss ways to build control protocols on the basis of ROMs. We illustrate several control protocols using the proposed method: in Sec. IV A, we discuss controllable information propagation across the system; in particular, we show the possibility of adjusting the quantum information transmission from Alice to Bob located at different ends of the chain. In Sec. IV B, we demonstrate the time reversal of the system dynamics. We summarize and discuss potential next steps in developing the proposed approach in Sec. V.

## II. BUILDING A REDUCED-ORDER MODEL

Consider a many-body quantum system that consists of two parts. Assume that the dynamics of the first part are of interest while the dynamics of the second part are not. This induces a natural separation of a many-body system into the target system ($S$) and the environment ($E$) in the spirit of the theory of open quantum systems. The system-environment Hilbert space reads $\mathcal{H} = \mathcal{H}_S \otimes \mathcal{H}_E$, where $\dim(\mathcal{H}_S) = d_S$, $\dim(\mathcal{H}_E) = d_E$. Our first goal is to build a low-dimensional effective model of the target system dynamics, whose numerical simulation is much simpler in comparison with the original model.

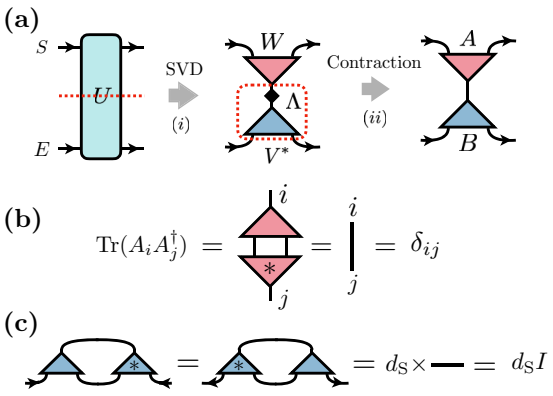


FIG. 1. (a) Two-step decomposition: (i) singular value decomposition of $U$, (ii) contraction of the lower isometric block with the diagonal matrix $\Lambda$. (b) Orthogonality relation for $A_i$. (c) Orthogonality relation for $B_i$.

For the sake of simplicity, we consider discretized time $t_n \in \{t_0, ..., t_N\}$, where $N$ consecutive time steps are equally spaced by $\tau$. Generalization of the proposed technique to the case of continuous time is also possible. For simplicity, we denote time-dependent quantities by the time-step index. Discrete-time dynamics of the joint system is driven by a unitary transformation $U : \mathcal{H}_S \otimes \mathcal{H}_E \to \mathcal{H}_S \otimes \mathcal{H}_E$, i.e., $|\psi(N)\rangle = U^N |\psi(0)\rangle$, where $|\psi(0)\rangle$ is an initial joint system-environment state. For simplicity, $|\psi(0)\rangle$ is supposed to factorize $|\psi(0)\rangle = |\psi_{SE}\rangle = |\psi_S\rangle \otimes |\psi_E\rangle$, nevertheless the generalization of the suggested approach to entangled initial states is straightforward.

Since the dynamics of the environment are not of interest, one can reduce its dimension in such a way that the dynamics of the target system remain almost the same. One needs to split $U$ into two parts to separate the system and environment. A unitary transformation $U$ can be represented as a four-way tensor, and its splitting between subsystems is determined by the dyadic decomposition

$$U = \sum_i A_i \otimes B_i, \tag{1}$$

which is defined via diagrammatic representation in Fig. 1(a). Both objects $A_i$ and $B_i$ are seen as three-way tensors, i.e., both have input and output physical indices and one internal index $i$ induced by decomposition. Note that one has the following orthogonality relation for $A_i$:

$$\mathrm{Tr}(A_i A_j^\dagger) = \delta_{ij}, \tag{2}$$

where $\delta_{ij}$ is the Kronecker delta. Diagrammatic representation of Eq. (2) is given in Fig. 1(b). One also has orthogonality relations for $B_i$,

$$\sum_i B_i^\dagger B_i = \sum_i B_i B_i^\dagger = d_S I, \tag{3}$$

where $I$ is the identity matrix. The diagrammatic interpretation of the expression Eq. (3) is given in Fig. 1(c). For the complete derivation of Eqs. (2) and (3), see Appendix A. The

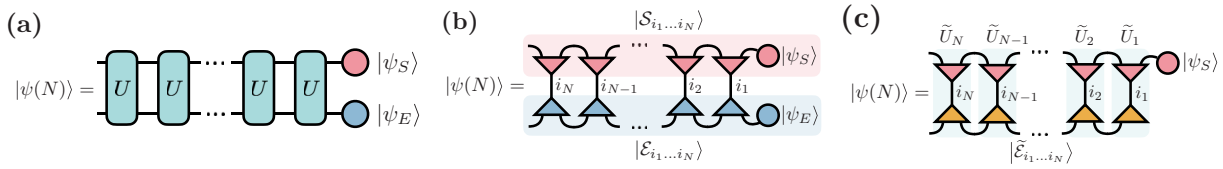


FIG. 2. (a) Representation of a coupled system and environment dynamics as a tensor network. (b) The same tensor network after decomposition. The entire network breaks up into a system network and an environment network shaded by red and grey regions correspondingly. (c) The truncated tensor network that approximates the exact system-environment dynamics.

most important consequence of these relations which we use further is that operator $K_i = \frac{1}{\sqrt{d_S}} B_i$ forms Kraus representation of a quantum channel, i.e., completely positive (CP) and trace-preserving (TP) map

$$\Phi[\cdot] = \sum_i K_i \cdot K_i^\dagger, \tag{4}$$

where the CP property is guarantied automatically and $\sum_i K_i^\dagger K_i = I$ guaranties the TP property.

Now let us use the dyadic decomposition Eq. (1) to represent the joint system and environment final state $|\psi(N)\rangle = U^N |\psi(0)\rangle$ as a tensor network necessary to proceed with the environment dimensionality reduction. The straightforward representation in terms of a tensor network is given in Fig. 2(a). Applying the decomposition Fig. 1(a) to all $U$ tensors in Fig. 2(a), one ends up with the tensor network Fig. 2(b). This tensor network can be split into two parts, a *system network* and an *environment network*; they read

$$\begin{aligned} |\mathcal{S}_{i_1\ldots i_N}\rangle &= A_{i_N} A_{i_{N-1}} \ldots A_{i_2} A_{i_1} |\psi_S\rangle , \\ |\mathcal{E}_{i_1\ldots i_N}\rangle &= B_{i_N} B_{i_{N-1}} \ldots B_{i_2} B_{i_1} |\psi_E\rangle . \end{aligned} \tag{5}$$

The final joint system and environment state in terms of networks $|\mathcal{S}_{i_1\ldots i_N}\rangle$ and $|\mathcal{E}_{i_1\ldots i_N}\rangle$ can be written as follows:

$$|\psi(N)\rangle = \sum_{i_1,\ldots,i_N} |\mathcal{S}_{i_1\ldots i_N}\rangle \otimes |\mathcal{E}_{i_1\ldots i_N}\rangle . \tag{6}$$

Note that both networks have a form almost identical to a matrix product state (MPS) [24,43], with the only difference in the last dangling edge. The environment network by construction describes all the environmental effects in the system's dynamics. By reducing its dimension, we end up with an effective low-dimensional environment network that leads to almost the same dynamics of the target system.

Due to the relations Eq. (3), the environment network is automatically in a so-called left-canonical form, which is the starting point of the standard MPS truncation algorithm [26,27,44]. This gives rise to an efficient environment network truncation technique equivalent to the standard MPS truncation algorithm. It is easy to formulate this technique purely regarding the environment dynamics induced by the quantum channel $\Phi$ introduced in Eq. (4). Consider the dynamics of the environment, starting from initial state $\varrho_E(0) = |\psi_E\rangle\langle\psi_E|$, under the action of the quantum channel $\Phi$, i.e.,

$$\varrho_E(n) = \Phi[\varrho_E(n-1)]. \tag{7}$$

The central and most important object is the spectrum $\lambda_1(n), \lambda_2(n), \ldots, \lambda_{d_E}(n)$ of $\varrho_E(n)$, where eigenvalues are arranged in the nonascending order. If the spectrum of $\varrho_E(n)$ is mostly concentrated in $r(n)$ largest eigenvalues, then $\varrho_E(n)$ can be effectively represented by its projection on a principal subspace that is the span of $r(n)$ dominant eigenvectors, i.e., eigenvectors with largest eigenvalues. This leads to the truncated version of the density matrix that reads

$$\tilde{\varrho}_E(n) = \pi(n)\varrho_E(n)\pi(n), \tag{8}$$

where $\pi(n)$ is the orthogonal projector on the principal subspace. Introducing a desirable error threshold $\sqrt{\sum_{j=r(n)+1}^{d_E} \lambda_j(n)} \leqslant \varepsilon_n$, one determines the principal subspace dimension $r(n)$ and the principal subspace itself as the column space of the matrix $\omega(n)$ whose columns are $r(n)$ dominant eigenvectors. The principal subspace is considered a low-dimensional effective environment Hilbert space at time step $n$. The details about the truncation technique and time-varying truncation effects are available in Appendix B. A formal algorithm with its reasoning is given in Appendix C.

To obtain the truncated environment network, it is enough to insert projection operators $\pi(n) = \omega(m)\omega^\dagger(m)$ in between neighboring blocks $B_{i_{n+1}}$ and $B_{i_n}$ for all $n$. This results in truncated blocks that read

$$\widetilde{B}_i^{(n)} = \begin{cases} \omega(n) B_i \omega^\dagger(n-1), & \text{for} \quad n > 1 \\ \omega(1) B_i |\psi_E\rangle , & \text{for} \quad n = 1, \end{cases} \tag{9}$$

and in the truncated environment, the network

$$|\widetilde{\mathcal{E}}_{i_1\ldots i_N}\rangle = \widetilde{B}_{i_N}^{(N)} \widetilde{B}_{i_{N-1}}^{(N-1)} \ldots \widetilde{B}_{i_2}^{(2)} \widetilde{B}_{i_1}^{(1)}. \tag{10}$$

By taking the convolution between the effective environment network and the system network, as it is sketched in Fig. 2(c), we get the effective low-dimensional model of the target system dynamics of time-depended dimension $\tilde{d}_n = d_S r(n)$. ROM is defined by effective gates $\widetilde{U}_m$ of size $d_S r(n) \times d_S r(n-1)$, driving joint dynamics of the system and the effective environment; they read

$$\widetilde{U}_n = \sum_i A_i \otimes \widetilde{B}_i^{(n)}. \tag{11}$$

The dynamics of the system with the use of ROM can be calculated as follows:

$$\tilde{\varrho}_S(n) = \mathrm{Tr}_E \left( \prod_{i=1}^{n} \widetilde{U}_i |\psi_S\rangle \langle\psi_S| \left[ \prod_{i=1}^{n} \widetilde{U}_i \right]^\dagger \right). \tag{12}$$

Note also that it is allowed to apply arbitrary control gates to the system. The presented approach requires operating with the exact environment, which could be computationally expensive for large systems. Indeed, the complexity of

truncation scales as $O(Nd_E^3)$ since it involves matrix decompositions and matrix multiplications per each time step. Thus, it is possible to truncate an environment whose dimension is about several thousand. To scale beyond this dimension, one can alternate the environment truncation described in this section and the iterative expansion of an environment. When an environment reaches a certain dimension, for example, several thousand, one truncates it and continues expanding it afterward. This allows us to avoid explicit operations with the exact environment. The iterative expansion procedure for chainlike environments is discussed in Sec. III A.

It is worth noting that the environment network is closely connected to an *influence functional* [45,46] that has been recently applied to a numerical simulation of quantum dynamics in a variety of contexts. The most widely spread use case of the influence functional is the numerical simulation of the dynamics of an open quantum system coupled with a harmonic bath. The early approach to this problem [47,48] cuts off long-time memory effects by removing multipliers from the exact analytical form of the influence functional of a harmonic bath, making it tractable for numerical treatment.

More recent approaches such as TEMPO [49] and its variations and improvements [50,51] use a low-rank tensor-network representation of the influence functional to improve accuracy and include long-time memory effects in the consideration. Another recent approach [52] aimed at replacing a complex harmonic bath with a simple one allowing numerical simulation of the system's dynamics. The core idea of the approach is to find such a surrogate bath, which has the same two-time correlation functions. In the case of a Gaussian bath, this is equivalent to the equality of influence functionals.

The combination of tensor network methods with influence functional theory is used to develop analytical and numerical methods for analyzing and modeling correlated spin systems. In particular, the self-consistency equation for the influence functional [40,42,53] allows one to study the long-time thermalized dynamics of spin systems both analytically and numerically. It has been shown that the influence functional admits exact disorder averaging [54], making it possible to study MBL phases rigorously.

Approaches based on the influence functional are especially successful in the case of irreversible processes with weak memory effects. In these cases, temporal entanglement is weak and a low-rank MPS can efficiently approximate an influence functional. Whereas such systems are fundamentally very interesting, they are not well controllable due to the high information loss rate. Systems with long memory effects and weak information loss are better controllable and more interesting from the optimal control perspective. For describing environmental effects in such kinds of problems, the environment network is better. To justify this claim, let us consider the connection of the environment network with the influence functional that is represented in Fig. 3. The environment network with bond dimension $r$ corresponds to the influence functional with bond dimension $r^2$. This means that the environment network can describe higher temporal entanglement and more complex memory effects. On the other hand, the environment network cannot efficiently describe irreversible loss of information. Any loss comes at the cost

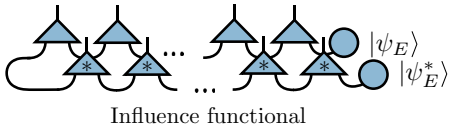


FIG. 3. Influence functional is a convolution of the environment network with the conjugated version of itself.

of increasing the bond dimension. Therefore, the environment network is well suited to describe processes that are well controllable, i.e., with small information loss and high temporal entanglement, and complements the influence functional based approaches. This motivates our choice of the environment network for optimal control purposes.

## III. MANY-BODY OPTIMAL CONTROL: METHODOLOGY

### A. Reduced-order modeling of a quantum spin chain

We begin validation of the proposed reduced-order modeling technique by building a ROM of XYZ quantum Heisenberg chain with an external magnetic field and open boundary conditions. The corresponding Hamiltonian is represented as a sum of local terms

$$H = \sum_{j=1}^{L-1} H_{j,j+1}, \tag{13}$$

where each local term includes spin-spin and local magnetic field interaction terms:

$$H_{j,j+1} = \sum_{\alpha\in\{x,y,z\}} J_\alpha \sigma_j^\alpha \sigma_{j+1}^\alpha + h_j \sigma_j^\alpha + h_{j+1}\sigma. \tag{14}$$

Here $\sigma_j^\alpha$, $\alpha \in \{x, y, z\}$ stands for Pauli matrix acting on a spin number $j$, $J_\alpha$ is a coupling constant, and $h_\alpha$ is a component of the external magnetic field. Spin chain dynamics can be discretized by a Suzuki-Trotter decomposition [55] and represented as a brickwork quantum circuit where each odd/even gate layer reads

$$U_O = \prod_{j=1}^{\lfloor (L-1)/2 \rfloor} \exp\left(-i\tau H_{2j,2j+1}\right),$$
$$U_E = \prod_{j=1}^{\lfloor L/2 \rfloor} \exp\left(-i\tau H_{2j-1,2j}\right), \tag{15}$$

where $\tau$ is a discretization step. This decomposition approximates the genuine Hamiltonian dynamics of a spin chain and becomes exact when $\tau \to 0$, $\tau N \to T$. Applying odd and even layers one after another to the initial state $|\psi(0)\rangle = \bigotimes_{i=1}^{L} |\psi_i\rangle$ of the spin chain leads to the final state shown in Fig. 4(a).

We can choose any spin in the chain as the target system, and consider the rest of the spin chain as an environment. Throughout the paper, we use $l$ to denote the target spin index. For large spin chains, the ROM building technique presented in Sec. II is not directly applicable, since it requires manipulations with the exact environment, whose dimension grows exponentially with the number of spins. However, the structure of the environment can be used, i.e., in this case,

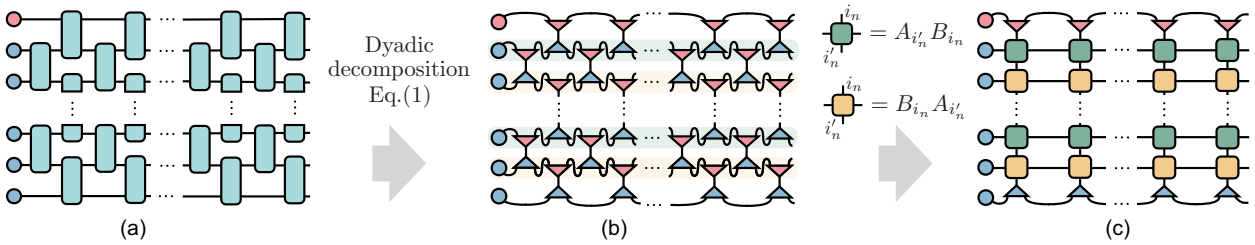


FIG. 4. (a) Tensor diagram of the Trotterized unitary evolution of spin chain. (b) Unitary evolution of spin chain after dyadic decomposition Eq. (1). (c) Unitary evolution of spin chain in terms of odd/even temporal MPOs.

it is either a chain connected to the edge spin or two chains connected to a spin inside. A key property of chainlike environments is that new spins can be recurrently added to the environment by simply inserting them between the current environment and the target system. This allows us to build an effective environment iteratively by adding one spin to the environment at a time and truncating the environment network using the algorithm from the Sec. II when the dimension reaches a threshold value. This approach is similar to the time-evolving block decimation algorithm [56], but instead of expanding the corresponding tensor network in the time domain, we expand it in space.

The procedure for constructing a ROM for a chainlike environment starts with the trotterization of the unitary dynamics of the joint system Fig. 4(a). Applying the dyadic decomposition Eq. (1) to a brickwork unitary circuit enables us to switch to another representation of joint system dynamics shown in Fig. 4(b). This representation makes it possible to identify a set of operators responsible for the dynamics of each spin in the chain separately. In this case, the interaction of spins is represented as a convolution of the corresponding operators resulting from Eq. (1).

Natural separation into even and odd layers in Suzuki-Trotter decomposition, after dyadic decomposition, leads to the appearance of two tensor subnetworks. These subnetworks are denoted $|O^{i'_1\ldots i'_N}_{i_1\ldots i_N}(k)\rangle$ for spin index $k = 1, 3, \ldots, \lfloor (L-1)/2 \rfloor$ and $|E^{i'_1\ldots i'_N}_{i_1\ldots i_N}(k)\rangle$ for spin index $k = 2, 4, \ldots, \lfloor L/2 \rfloor$. These subnetworks describe the dynamics of the environmental spins and can be represented as convolutions of operators resulting from the dyadic decomposition of the following form:

$$
\begin{aligned}
|E^{i'_1\ldots i'_N}_{i_1\ldots i_N}(k)\rangle &= A^{(k)}_{i'_N} B^{(k)}_{i_N} \ldots A^{(k)}_{i'_1} B^{(k)}_{i_1} |\psi_k(0)\rangle\,, \\
|O^{i'_1\ldots i'_N}_{i_1\ldots i_N}(k)\rangle &= B^{(k)}_{i_N} A^{(k)}_{i'_N} \ldots B^{(k)}_{i_1} A^{(k)}_{i'_1} |\psi_k(0)\rangle\,.
\end{aligned} \tag{16}
$$

Introducing two different types of elementary tensors $A^{(k)}_{i'_n} B^{(k)}_{i_n}$ and $B^{(k)}_{i_n} A^{(k)}_{i'_n}$, we can represent the joint system dynamics as shown in Fig. 4(c). We note that in this representation, subnetworks $|O^{i'_1\ldots i'_N}_{i_1\ldots i_N}(k)\rangle$ and $|E^{i'_1\ldots i'_N}_{i_1\ldots i_N}(k)\rangle$ can be seen as matrix product operators (MPOs) with only differences in the final dangling edge.

Using the introduced MPOs, we can describe the iterative procedure for constructing a ROM of a spin chain. First, we fix the dynamical subnetwork of the edge environmental spin. Because of the open boundary conditions, for the edge spin, this subnetwork has an MPS structure and can be interpreted as an environment network. Next, we iteratively add more subsystems to the environment network by performing MPS-MPO contraction,

$$
\begin{aligned}
&|\mathcal{E}_{i_1\ldots i_N}(k+1)\rangle \\
&= \begin{cases} \sum\limits_{i'_1,\ldots,i'_N} |E^{i'_1\ldots i'_N}_{i_1\ldots i_N}\rangle \otimes |\widetilde{\mathcal{E}}_{i'_1\ldots i'_N}(k)\rangle\,, & k+1-\text{even} \\ \sum\limits_{i'_1,\ldots,i'_N} |O^{i'_1\ldots i'_N}_{i_1\ldots i_N}\rangle \otimes |\widetilde{\mathcal{E}}_{i'_1\ldots i'_N}(k)\rangle\,, & k+1-\text{odd}, \end{cases}
\end{aligned} \tag{17}
$$

resulting in a new environment network $|\mathcal{E}_{i_1\ldots i_N}(k+1)\rangle$, which is fed into the truncation algorithm (Sec. II) if the environment dimension exceeds a threshold. The complete iteration of adding spin to the effective environment is illustrated in Fig. 5. Such an iterative approach does not require explicit manipulations with the complete environment and is therefore scalable and applicable to large chainlike environments. We also note that such an approach is applicable for general treelike interaction graphs.

We perform an iterative order reduction procedure and end up with an effective low-dimensional model describing the dynamics of the target spin. Such a construction can be built for the case of the arbitrary location of the target spin in the chain. The dynamics of the target spin $l$ within the ROM reads

$$
\begin{aligned}
|\tilde{\psi}(n)\rangle &= \widetilde{U}_n \ldots \widetilde{U}_2 \widetilde{U}_1 |\psi_l(0)\rangle\,, \\
\tilde{\varrho}_l(n) &= \mathrm{Tr}_E\big(|\tilde{\psi}(n)\rangle\langle\tilde{\psi}(n)|\big),
\end{aligned} \tag{18}
$$

where $|\tilde{\psi}_l(k)\rangle$ is the joint target spin and effective environment state at discrete time $n$ and $\varrho_l(n)$ is the state of the target spin. Note that in general case, the dimension $\tilde{d}_n = 2r(n)$ of $|\tilde{\psi}(n)\rangle$ increases with time because of the entanglement growth with

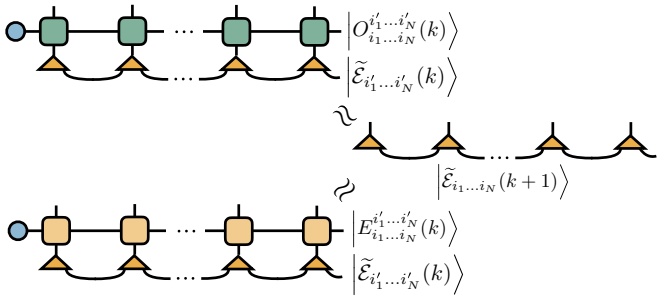


FIG. 5. Illustration of an elementary environment expanding step. Environment network in MPS form is contracted with an MPO of an additional (even/odd) spin. Next, if the threshold dimension is reached, truncation is performed, which gives a new MPS.

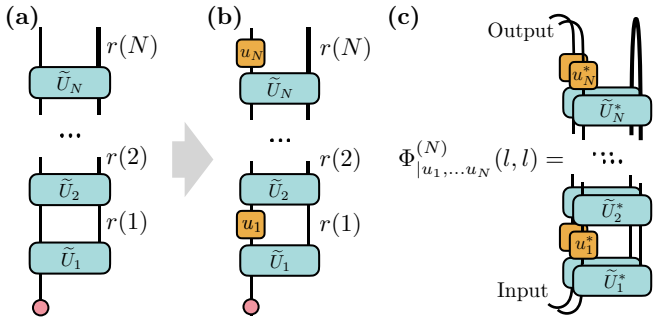


FIG. 6. (a) ROM describing dynamics of the edge spin. Varying edge thicknesses represent an increase of the effective environment dimension $\tilde{d}(n) = 2r(n)$ with time. (b) Tensor diagram showing how one applies control signal $\{u_1, \ldots, u_N\}$ to the target spin. (c) Tensor diagram representing the quantum channel driving the dynamics of the target spin in terms of ROM. Asterisk stands for complex conjugate.

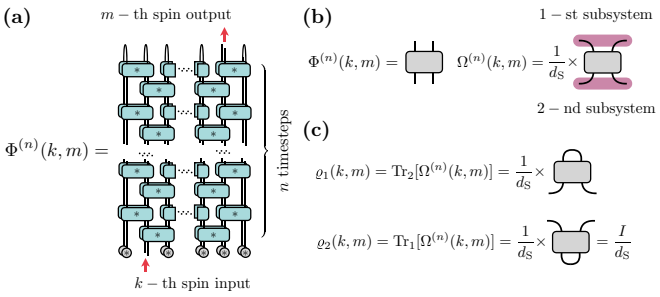


FIG. 7. (a) Diagrammatic representation of the quantum channel $\Phi^{(n)}(k, m)$. (b) Diagrammatic representation of the corresponding Choi matrix $\Omega^{(n)}(k, m)$. The only difference between $\Phi^{(n)}(k, m)$ and $\Omega^{(n)}(k, m)$ is in the multiplier $1/d_S$. (c) Diagrammatic representation of $\varrho_1^{(n)}(k, m)$ and $\varrho_2^{(n)}(k, m)$. Note that due to the TP property of $\Phi^{(n)}(k, m)$, $\varrho_2^{(n)}(k, m)$ is proportional to the identity operator.

time between target spin and spins of environment Fig. 6(a). Thus, the dynamics of the target spin, taking into account external control, in terms of ROM, can be represented as in Fig. 6(b), corresponding quantum channel shown in Fig. 6(c).

In the following section, we move forward and apply the developed reduced-order modeling scheme to various optimal control problems.

### B. Reduced-order modeling based optimal control

ROM techniques are well-suited for optimal control methods in many-body quantum physics. Indeed, the main difficulty towards efficient quantum many-body optimal control is the necessity of running dynamics simulations thousands of times. This difficulty is substantially mitigated via reduced-order modeling. The overall optimal control scheme breaks up into two steps:

(1) Build ROM of a quantum many-body system.

(2) Formulate an optimal control problem as an optimization problem in terms of ROM and solve it using some optimization algorithm.

It remains unclear what kind of optimization method to use. A typical control problem written in terms of the optimization problem takes the following form:

$$\min_{\{u_i\}_{i=1}^{\Delta n}} \mathcal{L}(u_1, \ldots, u_{\Delta n}),$$
$$\text{s.t. } u_i^\dagger u_i = I, \tag{19}$$

where $\mathcal{L}$ is the loss function in terms of ROM and measures how good a control signal is, $\{u_i\}_{i=1}^{\Delta n}$ is a $\Delta n$-step sequence of unitary control gates applied to the system, i.e., it is a control signal that needs to be optimized, and $I$ is the identity operator. Note that Eq. (19) is the constrained optimization problem. Since control gates are unitary, an optimization technique of our choice must preserve $u_i^\dagger u_i = I$ for all gates.

To solve the given optimization problem, we found a Riemannian optimization algorithm [57,58], namely, the Riemannian ADAM optimizer [59,60], to be efficient. It performs a gradient-based search of the optimal point on a manifold defined by the constraints, in our case on the manifold of unitary matrices (a special case of the complex Stiefel manifold [61–64]). We calculate the gradient of $\mathcal{L}$ with respect o $\{u_i\}_{i=1}^{\Delta n}$ utilizing the automatic differentiation technique [23]. The Riemannian ADAM optimizer performs a descent procedure towards the optimal point on the manifold of unitary matrices until convergence, evaluating the gradient of $\mathcal{L}$ typically around $10^4$ times. Note that without the use of ROM, even a single calculation of the gradient becomes extremely memory demanding since automatic differentiation requires keeping all intermediate data in memory.

### C. Information flows computation and visualization

To validate optimal control results and gain intuition behind them, it is instructive to visualize how information about the initial state of a certain spin propagates across a spin chain. For this purpose, we introduce a quantum channel $\Phi^{(n)}(k, m)$ that maps the initial state of the $k$th spin to the state of the $m$th spin at time step $n$. Its diagrammatic representation is given in Fig. 7(a). This quantum channel fully characterizes correlations between the initial state of the $k$th spin and the state of the $m$th spin at the $n$th discrete time moment. To quantify correlations by a single value, one can turn to the corresponding Choi matrix $\Omega^{(n)}(k, m)$ that is represented in terms of tensor diagrams in Fig. 7(b). This Choi matrix is seen as the density matrix of a two-component quantum system, and thus the mutual information between those components $\mathcal{I}^{(n)}(k, m)$ is well-defined and reads

$$\mathcal{I}^{(n)}(k, m) = S\big(\varrho_1^{(n)}(k, m)\big) + S\big(\varrho_2^{(n)}(k, m)\big) - S\big(\Omega^{(n)}(k, m)\big), \tag{20}$$

where $S$ stands for von Neumann entropy, $\varrho_1^{(n)}(k, m)$ is the first component density matrix and $\varrho_2^{(n)}(k, m)$ is the second component density matrix. Both $\varrho_1^{(n)}(k, m)$ and $\varrho_2^{(n)}(k, m)$ are represented in terms of tensor diagrams in Fig. 7(c). Mutual information $\mathcal{I}^{(n)}(k, m)$ is well-suited for our visualization purposes, showing how information about the $k$th spin propagates in discrete time $n$ and space $m$. Note that there are other quantities that maybetter suit for this role, e.g., quantum capacity [65–67], but mutual information is much easier to calculate.

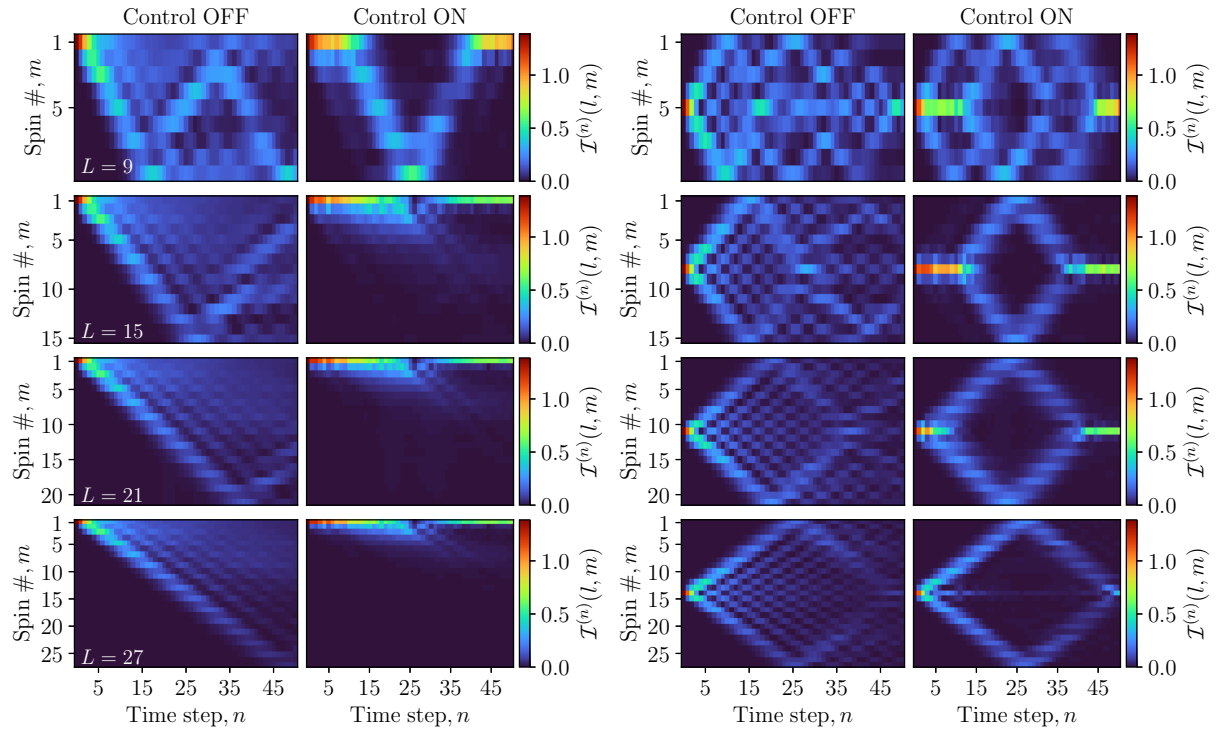


FIG. 8. Density plots representing dynamics of mutual information $\mathcal{I}^{(n)}(l, m)$ on a spin chain with turned ON/OFF control for $l$ being equal to 1 (left panel) and $\frac{n-1}{2} + 1$ (right panel).

## IV. MANY-BODY OPTIMAL CONTROL: NUMERICAL EXPERIMENTS

In this section, we describe several numerical experiments to demonstrate the performance of the approach. However, the possible applications of the proposed approach are not limited to those presented here.

### A. Controllable information propagation in a quantum spin chain

We start with examples of controllable information propagation in the XYZ model discussed in Sec. III A. We choose the following parameters of the model: $J_x = 0.9, J_y = 1, J_z = 1.1, h_x = 0.2, h_y = 0.2, h_z = 0.2, \tau = 0.15$, and the following initial states of the target spin and the environment:

$$|\psi_S\rangle = |\uparrow\rangle, \quad |\psi_E\rangle = \bigotimes_{i=1}^{L} |\downarrow\rangle. \tag{21}$$

Chosen model parameters correspond to weakly nonintegrable dynamics in the continuous in time case. Although we choose a special environment initial state, it is natural to expect qualitatively similar results after averaging over random environment initial states.

Within the first task, we consider a bit artificial but complicated control problem causing nontrivial information flow under optimal control. The problem is formulated as follows: Find a control sequence $\{u_1, \ldots, u_N\}$ applied to the target spin that $\varrho_l(0) = \varrho_l(N)$ and $\varrho_l(N/2) = \frac{I}{2}$, where $\varrho_l$ is the density matrix of the target spin. In other words, we want the information about the initial state of the target spin to be completely absorbed by the environment at time $\tau N/2$ and completely reconstructed back at the end of the time interval. This control problem has the following formulation in terms of optimization:

$$\min_{\{u_i\}_{i=1}^N} \left\| \Phi^{(N/2)}_{|u_1,\ldots,u_{N/2}}(l,l) - \Delta \right\|_F^2 + \left\| \Phi^{(N)}_{|u_1,\ldots,u_N}(l,l) - I \right\|_F^2$$
$$\text{s.t. } u_i^\dagger u_i = I, \text{ for } i \in \{1, \ldots, N\}, \tag{22}$$

where $\Phi^n_{|u_1,\ldots,u_n}(l,l)$ is a quantum channel that maps the initial state of a target spin $l$ to the state of the target spin at discrete time step $n$, $I$ is the identity quantum channel, $\Delta$ is a quantum channel that maps any state to the completely mixed state $\frac{1}{2}I$, and subscript $F$ stands for the Frobenius norm. We resolved this optimization problem using the technique from Sec. III B. We built ROM using an environment truncation scheme with truncation threshold $r_{\max} = 512$ and truncation accuracy $\varepsilon = 0.01$ (see Appendixes B and C for details).

We conduct the exact dynamics simulation under optimal control and without control to study how the information about the initial state of the target spin propagates in the spin chain. The information flow in all cases is visualized in Fig. 8.

One can see that the optimal control sequence achieves the desired information flow, i.e., at the intermediate time, information about the initial state of the target spin dissolves in the rest of the spin chain; however, at the end of the dynamics, it is concentrated back in the target spin. Note that the optimal control sequence uses reflection of the information flow from borders of the spin chain as a resource when possible, i.e., when the information flow has enough time to reflect from a border and get back. Note that this is an effect of many-

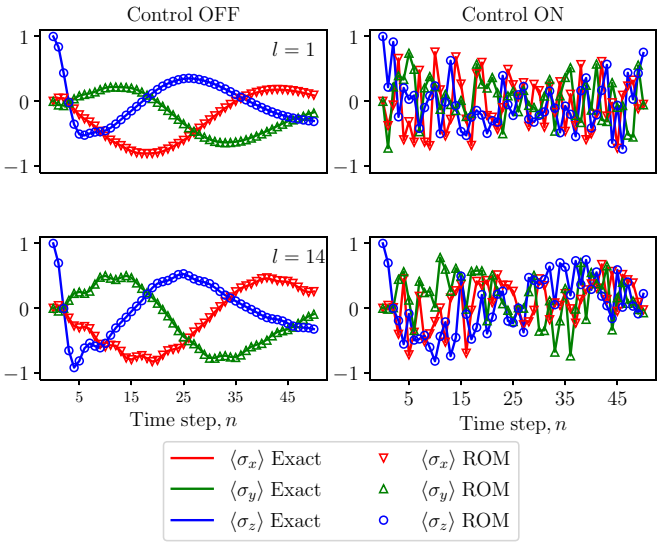


FIG. 9. Comparison of the exact and ROM-based dynamics for XYZ chain of $L = 27$ spins.

body echo, that is recognized and utilized by the optimization algorithm with only the use of the ROM. We also compare the exact dynamics of the target spin with the dynamics simulated by the use of the ROM in the case of a random external control signal to show that the ROM is capable of predicting the response to the external control signal. The results are given in Fig. 9.

We also study how the dimension of the ROM, i.e., $2r(k)$, scales with time for various numbers of spins. Figure 10 qualitatively demonstrates the effect of dimensionality reduction for the case of target spin fixed to be the edge spin. One can see that the dimension of the ROM grows much slower compared to the light-cone-based estimation of the effective dimension. While the ROM dimension for 27 spins reaches $\approx 10^4$ at the final time step, the light cone covers the entire spin chain. This is evidence of the proposed ROM technique efficiency because the naive light-cone-based estimation of the effective dimension results in $\tilde{d}_N \approx 2^{27} \approx 1.3 \times 10^8$ while the ROM technique results in $\tilde{d}_N \approx 10^4$.

Model reduction becomes intractable with increasing simulation time, since $r(k)$ grows exponentially, and one cannot simulate thermalization of the target spin. Nevertheless, the reduction technique is well-suited for different control problems simplification.

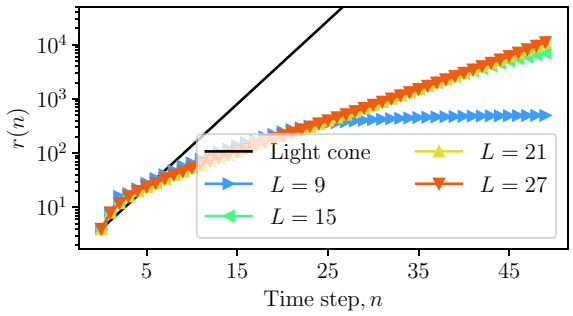


FIG. 10. Comparison of the ROM dimension with the light cone-based estimation of the effective dimension for different numbers of spins.

Within the second control problem, we apply the proposed method to design a control protocol for quantum information transfer through a spin chain. Let us assume that Alice prepares one of the spins in some state. The goal of Bob, who has access to one of the other spins, is to apply such a control sequence $\{u_1, \ldots, u_N\}$ to his spin, that after time $\tau N$ Bob has his spin in the state as close as possible to the initial state of Alice's spin. In other words, Bob has to catch information propagating from Alice and reconstruct the initial state. To formulate this task as an optimization problem, let us fix four quantum states of Alice's spin $\{|\phi_q\rangle\langle\phi_q|\}_{q=0}^3$. Corresponding Bloch vectors lie at the vertices of the tetrahedron, i.e., $|\phi_q\rangle\langle\phi_q| = \frac{1}{2}(I + \sum_k s_k^{(q)}\sigma_k)$, where $s_k^{(q)}$ are components of vectors $\{\mathbf{s}^{(q)}\}_{q=0}^3$ that read

$$\mathbf{s}^{(0)} = (0, 0, 1),\ \mathbf{s}^{(1)} = \left(\frac{2\sqrt{2}}{3}, 0, -\frac{1}{3}\right),$$

$$\mathbf{s}^{(2)} = \left(-\frac{\sqrt{2}}{3}, \sqrt{\frac{2}{3}}, -\frac{1}{3}\right), \mathbf{s}^{(3)} = \left(-\frac{\sqrt{2}}{3}, -\sqrt{\frac{2}{3}}, -\frac{1}{3}\right).$$

The ability to pass these four states, which define SIC-POVM, through the chain of spins from Alice to Bob is enough to pass an arbitrary spin state. For the fixed initial state of Alice's spin (in our case, $|\downarrow\rangle$) one can formulate the problem of transferring states $\{|\phi_q\rangle\langle\phi_q|\}_{i=0}^3$ through the spin chain as the following optimization problem:

$$\min_{\{u_i\}_{i=1}^N} \sum_{i=0}^{3} \| |\phi_q\rangle\langle\phi_q| - \Phi^{(N)}_{|u_1,\ldots,u_N}(l_A, l_B)\big[|\phi_q\rangle\langle\phi_q|\big]\|_F^2,$$

$$\text{s.t. } u_i^\dagger u_i = I \text{ for } i \in \{1, \ldots, N\}, \tag{23}$$

where $\Phi^{(N)}_{|u_1,\ldots,u_N}(l_A, l_B)[|\phi_q\rangle\langle\phi_q|]$ is the final state of Bob's spin given the initial state of Alice's spin and the control sequence, $l_A, l_B$—indices of Alice's and Bob's spins correspondingly.

For each initial state $|\phi_q\rangle$ of Alice's spin, we build a separate ROM describing dynamics of Alice's spin and utilize it to compute $\Phi^{(N)}_{|u_1,\ldots,u_N}(l_A, l_B)[|\phi_q\rangle\langle\phi_q|]$. The optimization problem Eq. (23) as previous ones is solved by using the technique from Sec. III B. To address the performance of the obtained optimal control sequence $\{u_1, \ldots, u_N\}$, we compare the initial states of Alice's spin with the final states of Bob's spins and study how the information about the initial state of Alice's spin propagates through the spin chain. The results are given in Fig. 11. An optimal control sequence applied to Bob's spin is able to partly reconstruct the initial state of Alice's spin. One can also observe how Bob catches the light cone that propagates from Alice's spin and preserves the information up to the end of the dynamics by using the optimal control sequence.

### B. Dynamics inversion via optimal control

Here we consider another quantum many-body optimal control problem. Suppose that one has access to a disordered spin system in the MBL phase [68–71] and it is allowed to

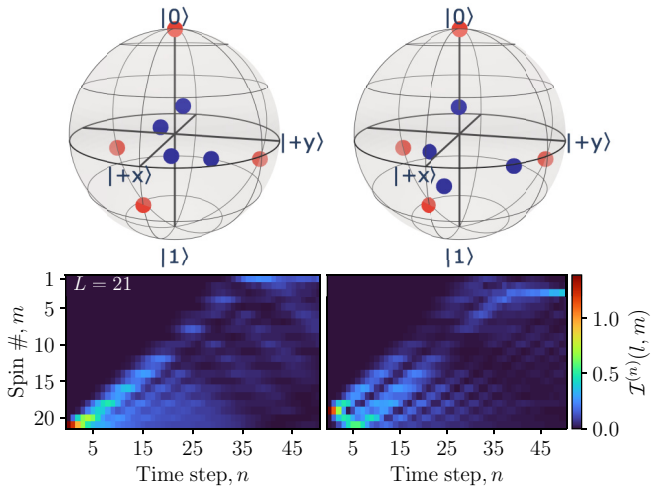


FIG. 11. Density plots represent how information about Alice's spin propagates through the spin chain. Points in the Bloch spheres show initial (red) and output (blue) states.

apply a control signal to a dedicated single spin. One needs to design such a control protocol that runs dynamics of this spin backward in time. A typical example of such a protocol is a spin-echo protocol [28,72] that runs dynamics backward in time in a sense that the controlled spin recovers information lost in the rest of the spin system after the spin-flip operation. Our goal is to design an alternative control protocol that leads to better information recovery. We start with a brief introduction to the origins of the spin-echo protocol in MBL systems. Following Refs. [72,73], this effect can be explained by the use of the phenomenological model of the MBL phase.

The MBL phase in the thermodynamic limit can be characterized by an infinite number of local integrals of motion, which can be thought of as effective spin-half operators $\tau_i^z$. In these terms, the MBL Hamiltonian takes the following form:

$$H_{\mathrm{MBL}} = \sum_i \tilde{h}_i \tau_i^z + \sum_{ij} \mathcal{J}_{ij} \tau_i^z \tau_j^z + \sum_{ijk} \mathcal{J}_{ijk} \tau_i^z \tau_j^z \tau_k^z + \ldots, \tag{24}$$

where couplings $\mathcal{J}_{ij}$, $\mathcal{J}_{ijk}, \ldots$ fall off exponentially with separation with a characteristic localization length $\xi$. All terms of this Hamiltonian commute with each other. Therefore, the total evolution operator $U_{\mathrm{MBL}}(t) = \exp(-itH_{\mathrm{MBL}})$ factorizes into the product of commuting exponents of individual terms. Considering one of those exponents that includes the participation of the first spin, it takes the following form:

$$\exp\left(-it\mathcal{J}_{1,i_2,\ldots,i_m}\tau_1^z\tau_{i_2}^z\ldots\tau_{i_m}^z\right) = \cos\left(t\mathcal{J}_{1,i_2,\ldots,i_m}\right) - i\sin\left(t\mathcal{J}_{1,i_2,\ldots,i_m}\right)\tau_1^z\tau_{i_2}^z\ldots\tau_{i_m}^z. \tag{25}$$

Taking into account the following relation:

$$\exp\left(-it\mathcal{J}_{1,i_2,\ldots,i_m}\tau_1^z\tau_{i_2}^z\ldots\tau_{i_m}^z\right)\tau_1^x = \tau_1^x\exp\left(it\mathcal{J}_{1,i_2,\ldots,i_m}\tau_1^z\tau_{i_2}^z\ldots\tau_{i_m}^z\right), \tag{26}$$

which follows from the Pauli algebra, one finally ends up with

$$U_{\mathrm{MBL}}(t)\tau_1^x U_{\mathrm{MBL}}(t)\tau_1^x = U_{\mathrm{MBL}/1}(2t), \tag{27}$$

where $U_{\mathrm{MBL}/1}$ denotes the MBL evolution operator that describes the MBL dynamics of all spins but the first spin and acts trivially (as the identity operator) on the first spin. If the MBL system evolves for some time $t$, then one applies the spin-flip control gate $\tau_x$ to the first spin, then the system evolves for the same time $t$ again, and finally one applies the spin-flip control gate $\tau_x$ to the first spin again, and ends up with the completely same state of the first spin as its initial state, i.e., the recovery of the information about the initial state of the first spin takes place. This is the essence of the spin-echo protocol. The same consideration is valid for an arbitrary spin from the system.

However, the phenomenological model Eq. (24) works well for the deeply localized phase. For the weakly localized phase, spin echo may barely be observed. Nevertheless, one can use the ROM-based optimal control technique from Sec. III B to design an alternative multistep spin-echo protocol suitable for a weakly localized phase. The multistep spin-echo protocol consists of the application of a sequence of unitary gates $\{u_1, \ldots, u_{\Delta n}\}$ instead of a single $\sigma_x$ gate, where $\Delta n$ is the duration of the protocol (number of control gates), to the target spin at the middle of the dynamics observation. We designed this protocol for one of the models experiencing MBL dynamics. The dynamics of this model are driven by the following Floquet operator [74]:

$$F = \exp\left[i\sum_{i=1}^{L} h_i\sigma_i^z + J\sigma_i^z\sigma_{i+1}^z\right]\exp\left[iJ\sum_{i=1}^{L}\sigma^x\right], \tag{28}$$

where per-spin magnetic fields are random and sampled from the uniform distribution Uniform$(0,\ 2\pi)$. The state of the whole system at discrete time $n$ reads $|\psi(n)\rangle = F^n|\psi(0)\rangle$.

It is known that this model is in the localized phase for $J < J^* \approx 0.4$ [74]. In this numerical experiment, we consider a system consisting of $n = 21$ spins, with coupling $J = 0.3$ corresponding to the localized phase, the target spin being the middle/edge spin, and compare the spin-echo-based dynamics inversion with a multistep spin-based dynamics inversion designed by the proposed technique. We set a particular quenched disorder, i.e., we picked a particular configuration of external magnetic fields from the distribution Uniform$(0,\ 2\pi)$.

We slightly generalized the spin-echo protocol to make it more suitable for a particular quenched disorder. Instead of the instant swap of the spin by $\sigma_x$ in the middle of the observation, we apply an instant unitary gate $u$ that is optimized to achieve the best performance by using the proposed method. In other words, the generalized version of the spin-echo protocol is the multistep spin-echo protocol of duration $\Delta n = 1$. As the initial state of the environment (all spins but the target spin), we take $|\psi_{\mathrm{E}}(0)\rangle = \bigotimes_{i=1}^{n-1}|\downarrow\rangle$. For the total number of discrete time steps $N = 151$, we built a ROM describing the dynamics of the target spin. For the multistep spin-echo protocol, we turn control ON in the time interval from $k_{\mathrm{start}} = 50$ to $k_{\mathrm{stop}} = 101$, i.e., the total protocol duration is $\Delta n = 51$ discrete time steps. For the spin-echo protocol, we turn the control ON only for the single discrete time moment $n = 76$.

To adjust the control signal to get the best echo effect at the end of the dynamics, one needs to formulate the control problem as the optimization problem. The

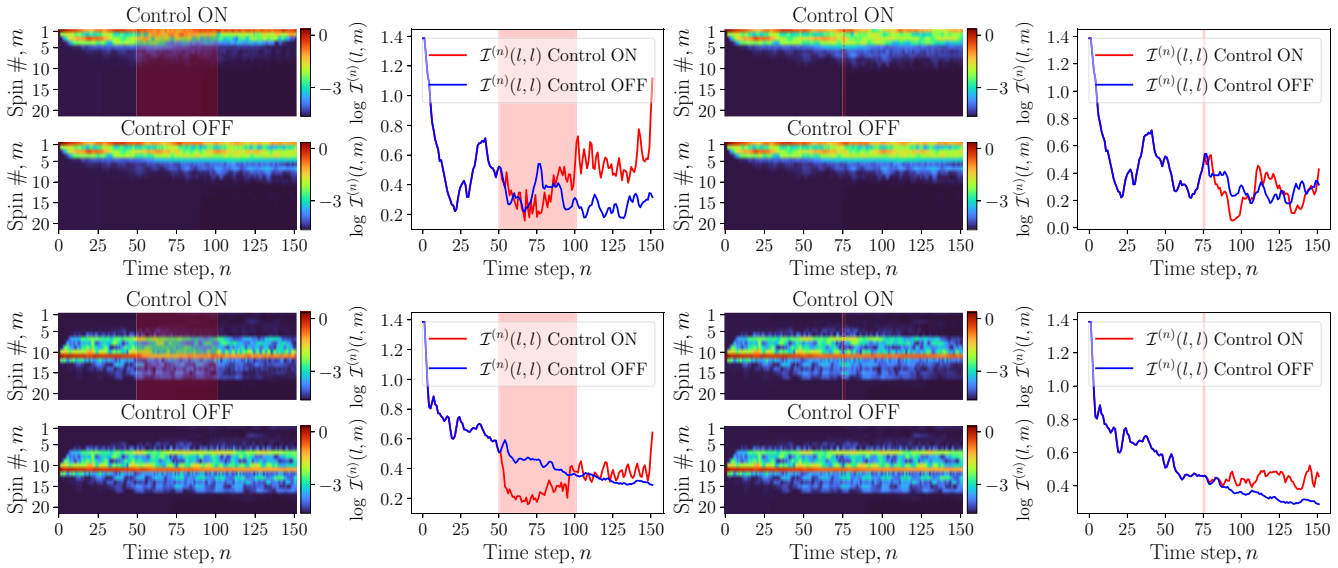


FIG. 12. Mutual information dynamics for $J = 0.3$. The top panel shows the results for the first spin being the target and the multi/single-step spin-echo protocol. The bottom panel shows the same with the middle spin being the target. Density plots represent how the rescaled mutual information $\ln(\mathcal{I}^{(n)}(l,m) + 10^{-2})$ propagates across the spin chain. The vertical red band represents a region in the time domain where the control sequence is applied.

initial and the final states of the target spin are connected via the quantum channel $\Phi^{(N)}_{|u_1,\ldots,u_{\Delta n}}(l,l)$ that can be defined by means of the ROM. The closer $\Phi^{(N)}_{|u_1,\ldots,u_{\Delta n}}(l,l)$ is to some unitary channel, the better echo effect one has. The mutual information $\mathcal{I}^{(N)}_{|u_1,\ldots,u_{\Delta n}}(l,l)$ between subsystems of the corresponding Choi matrix $\Omega^{(N)}_{|u_1,\ldots,u_{\Delta n}}(l,l)$ reaches its maximum when $\Phi^{(N)}_{|u_1,\ldots,u_{\Delta n}}(l,l)$ is a unitary channel. Thus, maximizing $\mathcal{I}^{(N)}_{|u_1,\ldots,u_{\Delta n}}(l,l)$, one maximizes the echo effect. Therefore, the solution of the following optimization problem provides the optimal control signal:

$$\max_{\{u_1,\ldots,u_{\Delta n}\}} \mathcal{I}^{(N)}_{|u_1,\ldots,u_{\Delta n}}(l,l),$$
$$\text{s.t. } u_i^\dagger u_i = I. \tag{29}$$

This optimization problem is solved by using the technique from Sec. III B.

After getting the optimal control sequence, for both protocols, we also run an exact simulation of the entire spin chain to study the information flow under control and compare protocols with each other and with the case of control absence. Using the results of the exact simulation, we visualized information flow showing how the information about the initial state of the target spin spreads across the spin chain. The results are given in Fig. 12.

The three main conclusions could be made out of Fig. 12. First, we observe the information revival at the end of the evolution for both spin-echo and multistep spin-echo protocols. This means that information about the initial target spin state is being reconstructed at the end of the evolution. Second, by looking at the density plots, we note that in the second half of the evolution, information about the initial target spin state starts to propagate backward toward the target spin for both control protocols. This implies that the dynamics inversion takes place. Finally, one can see that the multistep spin echo protocol outperforms the spin echo protocol in terms of revival amplitude. Therefore, the multistep spin-echo protocol works better than the standard spin echo protocol.

To check that the conclusions above are still valid after averaging over disorder, we performed averaging over ten different disorder realizations for $J = 0.2$ and all other parameters being the same. The same plots but for averaged quantities are shown in Fig. 13. All the features we observed for a particular disorder realization are also valid on average.

As opposed to the model considered in Sec. IV A, many-body dynamics in the localized phase do not exhibit ballistic trajectories. For this reason, the truncation procedure leads to an even slower dimension growth of the ROM. ROM dimension scaling is shown in Fig. 14.

## V. DISCUSSION AND OUTLOOK

In the present paper, we have proposed a method for many-body quantum control that is based on the ROM scheme accelerating a numerical simulation of many-body quantum systems in many orders of magnitude. This acceleration makes it possible to run tens of thousands of iterations of a gradient-based control signal search in a reasonable total time. We have validated the proposed method on the number of control problems, including controllable information spreading across a spin chain and dynamics inversion in the MBL phase.

The proposed method gives rise to a unique class of many-body control methods. Their field of applications varies from the development of methods of error mitigation and noise suppression in quantum technologies to an automatic search for unique quantum materials, phases of matter, and collective effects in many-body physics.

The proposed method can be generalized in various ways. For instance, instead of the iterative scheme for building the

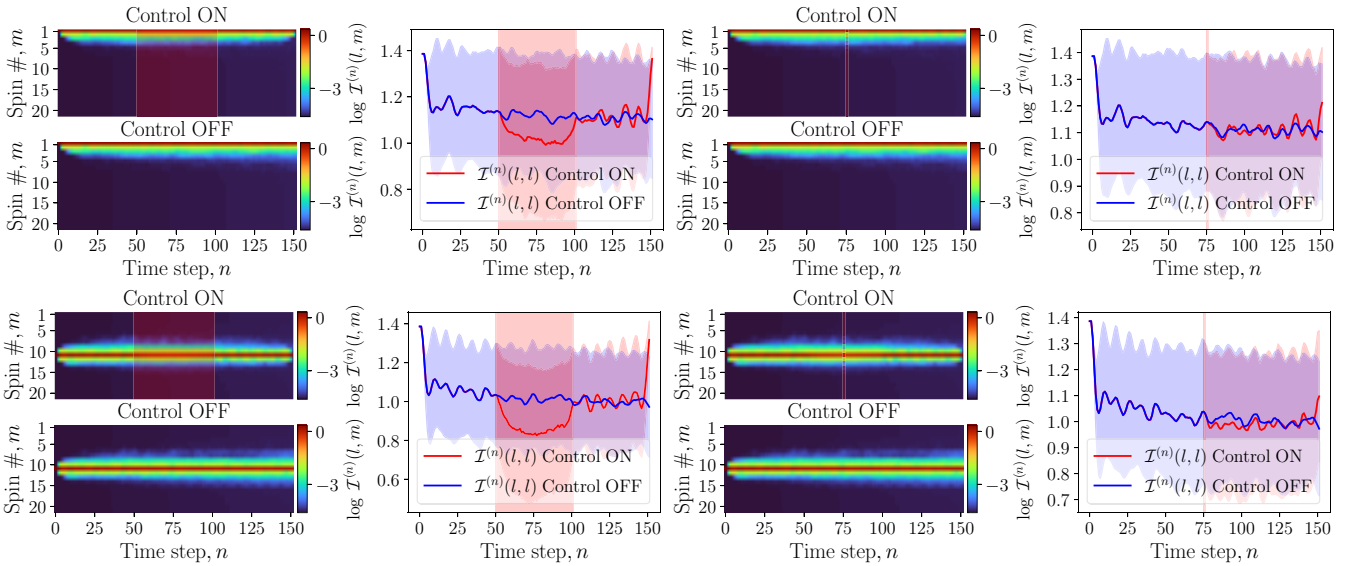


FIG. 13. Mutual information dynamics averaged over 50 disorder realizations for $J = 0.2$ Top panel shows the results for the first spin being the target and the multi/single-step spin-echo protocol. The bottom panel shows the same with the middle spin being the target. Density plots represent rescaled averaged mutual information $\ln(\langle\mathcal{I}^{(n)}(l,m)\rangle + 10^{-2})$. The vertical red band represents a region in the time domain where the control sequence is applied. Blue and red plotted regions represent the dispersion of mutual information over disorder realizations.

effective environment proposed in the paper, one can use tensor network renormalization techniques such as those introduced in Refs. [75–79]. Such methods potentially can be used to obtain ROMs of environments with 2D interaction graphs by renormalization instead of iterative growing.

Another possible generalization lies in the transition from the control of local observables and partial density matrices to macroscopic observables, e.g., total energy, total polarization, etc. Indeed, together with the environment dimensionality reduction one can renormalize macroscopic observables leading to ROMs of macroscopic observables dynamics. This opens possibilities for steering quantum many-body systems between different phases of matter via external control. The transition from local to macroscopic is possible not only for observables but also for control signals. For instance, instead of applying a control signal to a single spin, one may want to apply the same time-dependent magnetic field to all spins. In this case, the design of the ROM is definitely more involved, but with the great development of the tensor networks toolbox, it may be possible.

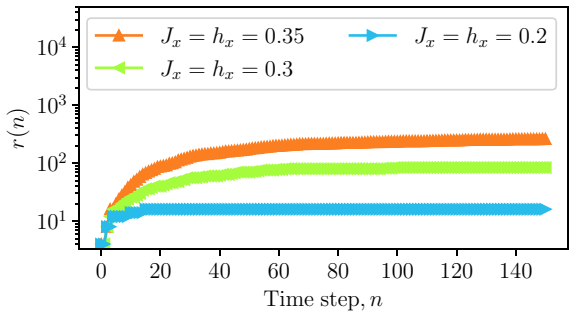


FIG. 14. ROM dimension vs time behavior for different couplings. The model becomes more complex approaching the transition at $J^* \approx 0.4$.

The next interesting generalization consists of the extraction of a ROM from observed experimental data. It is often the case that one has access to an experimental setup with the possibility to measure the response of a quantum system of interest on an external control signal. The question is whether it is possible to build the ROM of a system of interest in this case based purely on observed data. With use of algorithms such as tensor-train cross approximation [26], one can try to do that efficiently and adaptively. Finally, the presented approach can be improved by unifying it with the influence matrix approach [40–42], allowing one to simulate long-time subsystem dynamics. The great development of tensor networks and dimensionality reduction techniques makes it possible to unify all further generalizations of the proposed method into a universal framework opening great possibilities for the automatic discovery of unique quantum devices, phases of matter, and quantum collective phenomena.

The code for all the numerical experiments is available via [80].

## ACKNOWLEDGMENTS

I.A.L., M.A.G., and A.K.F. acknowledge support by the RSF Grant No. 19-71-10092 (studies of the many-body control approach) and the Priority 2030 program at the National University of Science and Technology (MISIS) under the Project No. K1-2022-027 (applications to spin chains).

## APPENDIX A: BUILDING A REDUCED-ORDER MODEL: ORTHOGONALITY RELATIONS

This Appendix is dedicated to giving the complete derivation of the introduced orthogonality relations. First, let us

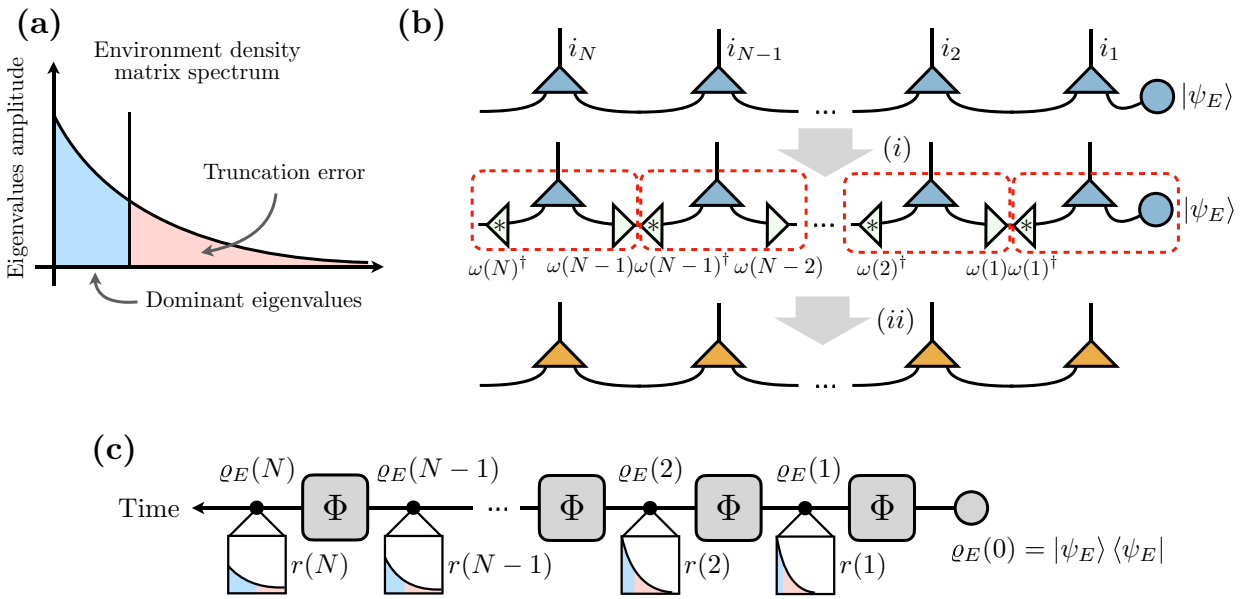


FIG. 15. (a) A typical spectrum of the environment density matrix. The tail of this spectrum contains only a tiny fraction of the total eigenvalues "mass" and thus can be truncated. (b) The environment truncation scheme: (i) One inserts projectors $\omega(n)\omega^\dagger(n)$ on the principal subspace in between of blocks forming the environment network. (ii) One contracts tensors in dashed red boxes and ends up with new yellow blocks that form a truncated environment network. (c) A typical time evolution of the environment density matrix spectrum. It gets wider in time and therefore the principal subspace dimension $r(n)$ grows in time.

discuss the orthogonality relation for $A_i$, Eq. (2). Indeed, the core of the decomposition Fig. 1(a) is the singular value decomposition (SVD) and Eq. (2) follows directly from the definition of SVD. To determine orthogonality relations for $B_i$, we consider the following relation:

$$\mathrm{Tr}_\mathrm{S}(UU^\dagger) = \mathrm{Tr}_\mathrm{S}(I \otimes I) = d_\mathrm{S} I, \tag{A1}$$

where $\mathrm{Tr}_\mathrm{S}$ is the partial trace over the system and $I$ is the identity matrix. On the other hand, one can make use of the decomposition Fig. 1(a) and Eq. (2) and rewrite $\mathrm{Tr}_\mathrm{S}(UU^\dagger)$ as follows:

$$\begin{aligned}\mathrm{Tr}_\mathrm{S}(UU^\dagger) &= \sum_{ij} \mathrm{Tr}_\mathrm{S}(A_i A_j^\dagger \otimes B_i B_j^\dagger) \\ &= \sum_{ij} \mathrm{Tr}(A_i A_j^\dagger) B_i B_j^\dagger \\ &= \sum_{ij} \delta_{ij} B_i B_j^\dagger = \sum_i B_i B_i^\dagger.\end{aligned} \tag{A2}$$

Gathering all together, one ends up with

$$\sum_i B_i B_i^\dagger = d_\mathrm{S} I. \tag{A3}$$

Considering $\mathrm{Tr}_\mathrm{S}(U^\dagger U)$ instead of $\mathrm{Tr}_\mathrm{S}(UU^\dagger)$, one also ends up with

$$\sum_i B_i^\dagger B_i = d_\mathrm{S} I, \tag{A4}$$

completing the proof of Eq. (3).

## APPENDIX B: BUILDING A REDUCED-ORDER MODEL: TRUNCATION

In this section, we discuss the details of the environment dimensionality reduction. To gain more intuition about how the principal subspace is determined, we schematically plotted a typical spectrum in Fig. 15(a). The relative error of the projection (truncation) reads

$$\frac{\|\tilde{\varrho}_\mathrm{E}(n) - \varrho_\mathrm{E}(n)\|_F}{\|\varrho_\mathrm{E}(n)\|_F} = \sqrt{\sum_{j=r(n)+1}^{d_\mathrm{E}} \lambda_j(n)}, \tag{B1}$$

where $F$ stands for the Frobenius norm. In other words, it means that the error is equal to the square root of the "mass" of eigenvalues in the spectrum tail that is cut and colored by red in Fig. 15(a).

Typically, $\varrho_\mathrm{E}(n)$ gets noiser in time, i.e., its spectrum gets wider. To preserve the truncated spectrum tail mass the same, one needs to increase $r(n)$ with time. Therefore, $r(n)$ typically grows in time. This is schematically illustrated in Fig. 15(b), where one can see how $r(n)$ grows with $n$ due to the widening of the spectrum.

The error introduced by the whole truncation procedure is bounded above as follows (see Appendix C and Ref. [27]):

$$\frac{\big\| |\widetilde{\mathcal{E}}_{i_1\ldots i_N}\rangle - |\mathcal{E}_{i_1\ldots i_N}\rangle \big\|_F}{\| |\mathcal{E}_{i_1\ldots i_N}\rangle \|_F} \leqslant \sqrt{\sum_{n=1}^{N} \varepsilon_n^2}. \tag{B2}$$

Therefore, if one requires the error to be less or equal to some upper bound $\varepsilon$ it is enough to set $\varepsilon_n = \frac{\varepsilon}{\sqrt{N}}$, which leads to

$$\frac{\big\| |\widetilde{\mathcal{E}}_{i_1\ldots i_N}\rangle - |\mathcal{E}_{i_1\ldots i_N}\rangle \big\|_F}{\| |\mathcal{E}_{i_1\ldots i_N}\rangle \|_F} \leqslant \varepsilon. \tag{B3}$$

Varying the value of $\varepsilon$, one achieves a trade-off between accuracy of approximation and effective environment dimension $r(n)$.

**Algorithm 1** Environment dimensionality reduction

**Require:** CPTP map $\Phi$, tensor $B_i$ forming the environment network, initial state $|\psi_{\mathrm{E}}\rangle$ of the environment, accuracy $\varepsilon$ of the algorithm
**Ensure:** The set of tensors $\{\widetilde{B}_i^{(m)}\}_{m=1}^{N}$ forming the reduced environment
1: Set the initial density matrix of the environment $\varrho(0) = |\psi_{\mathrm{E}}\rangle\langle\psi_{\mathrm{E}}|$ and the initial isometry $w(0) = |\psi_{\mathrm{E}}\rangle$
2: **for** $m \leftarrow 0$ to $N-1$ **do**
3: Propagate the density matrix of the environment forward in time: $\varrho(m+1) = \Phi[\varrho(m)]$
4: Perform eigendecomposition of $\varrho(m+1)$: $U(m+1)\Lambda(m+1)U^{\dagger}(m+1) = \varrho(m+1)$
5: Calculate the minimal environment dimension $r(m+1)$ that suits the given error upper bound $\epsilon$: $r(m+1) = f(\epsilon, \{\lambda_j(m+1)\}_{j=1}^{d_{\mathrm{E}}})$
6: Truncate the density matrix rank $\varrho(m+1) \leftarrow U_{r(m+1)}(m+1)\Lambda_{r(m+1)}(m+1)U^{\dagger}_{r(m+1)}(m+1)$
7: Calculate the next isometry $w(m+1)$: $w(m+1) = U_{r(m+1)}(m+1)$
8: Calculate the next tensor $\widetilde{B}_i^{(m+1)}$: $\widetilde{B}_i^{(m+1)} = w^{\dagger}(m+1)B_i w(m)$
9: **end For**

## APPENDIX C: BUILDING A REDUCED-ORDER MODEL: ALGORITHM AND ITS RATIONALE

In this Appendix, we justify the proposed environment network dimensionality reduction algorithm and provide its precise formulation.

First, we discuss the dimensionality reduction of the environment network at a specific discrete time moment. Let $|\mathcal{E}^{(m)}_{i_1\ldots i_N}\rangle$ be the environment network whose dimension at a discrete time moment $m$ has been reduced, i.e.,

$$\left|\mathcal{E}^{(m)}_{i_1\ldots i_N}\right\rangle = B_{i_N}\ldots B_{i_{m+1}} w(m)w^{\dagger}(m)B_{i_m}\ldots B_{i_1}|\psi_{\mathrm{E}}\rangle\,, \tag{C1}$$

where $w(m)$ is a trial isometric matrix of size $d_{\mathrm{E}} \times r(m)$, and $r(m)$ is a new environment dimension such that $r(m) < d_{\mathrm{E}}$. A natural choice of $w(m)$ is the one that leads to the minimal error, i.e., we require $w(m)$ to be the solution of the following optimization problem:

$$\begin{aligned} &\min_{w(m)} \left\| \left|\mathcal{E}^{(m)}_{i_1\ldots i_N}\right\rangle - |\mathcal{E}_{i_1\ldots i_N}\rangle \right\|_F^2, \\ &\text{s.t. } w^{\dagger}(m)w(m) = I, \end{aligned} \tag{C2}$$

where the Frobenius norm is taken over all indices, i.e., the "physical" index and the set of indices $\{i_1, \ldots, i_N\}$. The objective function $\mathcal{F}(\omega(m)) = \| |\mathcal{E}^{(m)}_{i_1\ldots i_N}\rangle - |\mathcal{E}_{i_1\ldots i_N}\rangle \|_F^2$ dramatically simplifies if one makes use of the property Eq. (3) and the introduced in Eq. (4) quantum channel $\Phi$. The simplified objective function takes the following form:

$$\mathcal{F}(\omega(m)) = d_{\mathrm{S}}^N\left(1 - \mathrm{Tr}\left(w^{\dagger}(m)\varrho_{\mathrm{E}}(m)w(m)\right)\right), \tag{C3}$$

where $\varrho_{\mathrm{E}}(m) = \Phi^m[|\psi_{\mathrm{E}}\rangle\langle\psi_{\mathrm{E}}|]$. Under the given constraints, this optimization problem is equivalent to the problem of finding $r(m)$ eigenvectors of $\varrho(m)$ corresponding to $r(m)$ maximal eigenvalues, i.e., the optimal $w(m)$ is the matrix whose columns are eigenvectors of $\varrho_{\mathrm{E}}(m)$ corresponding to $r(m)$ largest eigenvalues. In other words, the optimal orthogonal projector $\pi(m) = w(m)w^{\dagger}(m)$ is the projector on $r(m)$ leading eigenvectors of $\varrho(m)$.

Another question that arises here is how one can one determine $r(m)$. In practice, one usually has some desirable approximation accuracy (admissible error). Let us connect this accuracy and $r(m)$. The relative error induced by the dimensionality reduction reads

$$\begin{aligned} \varepsilon_m &= \frac{\left\| |\mathcal{E}^{(m)}_{i_1\ldots i_N}\rangle - |\mathcal{E}_{i_1\ldots i_N}\rangle \right\|_F}{\| |\mathcal{E}_{i_1\ldots i_N}\rangle \|_F} \\ &= \sqrt{\sum_{j=r(m)+1}^{d_{\mathrm{E}}} \lambda_j(m)}. \end{aligned} \tag{C4}$$

The above relation for the error allows one to determine the minimal value of $r(m)$ that suits some desirable accuracy $\varepsilon_m$ as a function $r(m) = f(\varepsilon_m, \{\lambda_j(m)\}_{j=1}^{d_{\mathrm{E}}})$ of eigenvalues and $\varepsilon_m$. We do not provide a concrete form of $f$ here for the case of a single time step dimensionality reduction but do this later for the case of all time steps.

This scheme can be applied to the environment network multiple times leading to an algorithm allowing dimensionality reduction for all time steps. The overall algorithm reads

This algorithm results in the truncated environment network $|\widetilde{\mathcal{E}}_{i_1\ldots i_N}\rangle$ that reads

$$|\widetilde{\mathcal{E}}_{i_1\ldots i_N}\rangle = w(N)\widetilde{B}^{(N)}_{i_N}\widetilde{B}^{(N-1)}_{i_{N-1}}\ldots\widetilde{B}^{(2)}_{i_2}\widetilde{B}^{(1)}_{i_1} \tag{C5}$$

Note, that one can omit $w(N)$ in the expression above. Indeed, we are not interested in the final state of the environment, we only care about the action of the environment on the system, i.e., the exact coincidence of environment networks is redundant; it is enough to have a coincidence of discretized Feynman-Vernon influence functionals [40–42,45] that are easily expressed through environment networks:

$$\langle\widetilde{\mathcal{E}}_{j_1\ldots j_N}|\widetilde{\mathcal{E}}_{i_1\ldots i_N}\rangle \approx \langle\mathcal{E}_{j_1\ldots j_N}|\mathcal{E}_{i_1\ldots i_N}\rangle\,. \tag{C6}$$

Due to the property $w^{\dagger}(N)w(N) = I$ matrix $w(N)$ does not affect the value of $\langle\widetilde{\mathcal{E}}_{j_1\ldots j_N}|\widetilde{\mathcal{E}}_{i_1\ldots i_N}\rangle$ and can be safely omitted.

It is important to note that the algorithm above is equivalent to the standard algorithm for MPS truncation [26,27,44]. The orthogonality relation $\sum_i B_i^{\dagger}B_i = d_{\mathrm{S}}I$ means that the environment network is in the left-canonical form that is the starting

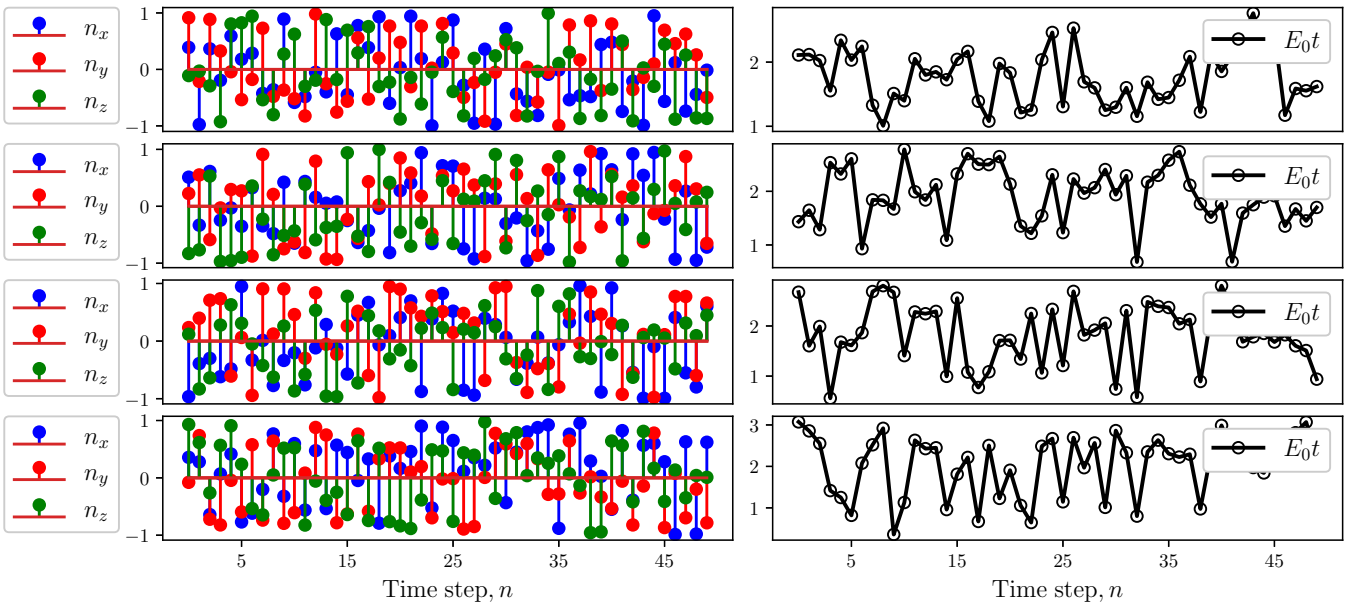


FIG. 16. Example of typical unitary control sequence.

point of the standard MPS truncation algorithm. By forwarding the environment density matrix in discrete time via CPTP map $\Phi$, we push the orthogonality center from the right side to the left. The projection on the leading eigenvectors of the environment density matrix is equivalent to the SVD-based truncation.

Finally, let us determine the function $f$. The error introduced by the entire algorithm is bounded above as follows [27]:

$$\varepsilon = \frac{\| |\widetilde{\mathcal{E}}_{i_1 \ldots i_N}\rangle - |\mathcal{E}_{i_1 \ldots i_N}\rangle \|_F}{\| |\mathcal{E}_{i_1 \ldots i_N}\rangle \|_F} \leqslant \sqrt{\sum_{n=1}^{N} \varepsilon_m^2}, \tag{C7}$$

where $\varepsilon_m$ is the error of $m$th time step dimensionality reduction. Therefore, restricting the one-time-step dimensionality reduction error $\varepsilon_m \leqslant \frac{\varepsilon}{\sqrt{N}}$, we guarantee that the error introduced by the entire algorithm does not exceed $\varepsilon$. This leads to the concrete form of the function $f$ guaranteeing a given accuracy $\varepsilon$ of the algorithm,

$$\begin{aligned} r(m) &= f\left(\varepsilon, \{\lambda_j(m)\}_{j=1}^{d_E}\right) \\ &= d_E - \sum_{r=1}^{d_E} \eta\left(\frac{\varepsilon}{\sqrt{N}}, \sqrt{\sum_{j=r+1}^{d_E} \lambda_j(m)}\right), \end{aligned} \tag{C8}$$

where $\eta$ is defined as follows:

$$\eta(x, y) = \begin{cases} 1, & \text{if } x > y \\ 0, & \text{otherwise.} \end{cases} \tag{C9}$$

## APPENDIX D: OPTIMAL UNITARY CONTROL

In this Appendix, we supplement the details of the results of the control optimization procedure. Control sequence optimization ends up with the sequence $\{u_1, \ldots, u_{\Delta n}\}$ of unitary control gates. Discarding the global phase, each unitary in this sequence can be written as

$$u = \cos(E_0 t) I - i \sin(E_0 t)(\vec{n}, \vec{\sigma}), \tag{D1}$$

where $\vec{n} = (n_x, n_y, n_z)$, $||\vec{n}|| = 1$, and $\vec{\sigma} = (\sigma_x, \sigma_y, \sigma_z)$. In the Bloch sphere picture, this corresponds to a rotation around the axis $\vec{n}$ at rate $E_0$. Since our control technique can be viewed as an instantaneous action of unitary control on each time step, we show $E_0 t$ and $\vec{n}$ in Fig. 16 to bring more information. The plotted control sample corresponds to the case of controllable information propagation considered in Sec. IV A, with results shown in Fig. 8 in the left panel.

[1] S. J. Glaser, U. Boscain, T. Calarco, C. P. Koch, W. Köckenberger, R. Kosloff, I. Kuprov, B. Luy, S. Schirmer, T. Schulte-Herbrüggen, D. Sugny, and F. K. Wilhelm, Training Schrödinger's cat: quantum optimal control, Eur. Phys. J. D **69**, 279 (2015).

[2] C. Altafini and F. Ticozzi, Modeling and control of quantum systems: An introduction, IEEE Trans. Autom. Control **57**, 1898 (2012).

[3] C. Altafini, Controllability properties for finite dimensional quantum Markovian master equations, J. Math. Phys. **44**, 2357 (2003).

[4] A. Borzì, Quantum optimal control using the adjoint method, Nanoscale Syst.: Math. Model. Theory Appl. **1**, 93 (2012).

[5] C. Brif, R. Chakrabarti, and H. Rabitz, Control of quantum phenomena: past, present and future, New J. Phys. **12**, 075008 (2010).

[6] S. Cong, *Control of Quantum Systems: Theory and Methods* (John Wiley & Sons, Hoboken, New Jersey, USA, 2014).

[7] D. Dong and I. R. Petersen, Quantum control theory and applications: a survey, IET Control Theory Appl. **4**, 2651 (2010).

[8] A. K. Fedorov, N. Gisin, S. M. Beloussov, and A. I. Lvovsky, Quantum computing at the quantum advantage threshold: a down-to-business review, arXiv:2203.17181.

[9] T. Caneva, T. Calarco, and S. Montangero, Chopped random-basis quantum optimization, Phys. Rev. A **84**, 022326 (2011).

[10] P. Doria, T. Calarco, and S. Montangero, Optimal control technique for many-body quantum dynamics, Phys. Rev. Lett. **106**, 190501 (2011).

[11] T. Caneva, A. Silva, R. Fazio, S. Lloyd, T. Calarco, and S. Montangero, Complexity of controlling quantum many-body dynamics, Phys. Rev. A **89**, 042322 (2014).

[12] S. van Frank, M. Bonneau, J. Schmiedmayer, S. Hild, C. Gross, M. Cheneau, I. Bloch, T. Pichler, A. Negretti, T. Calarco *et al.*, Optimal control of complex atomic quantum systems, Sci. Rep. **6**, 34187 (2016).

[13] F. Metz and M. Bukov, Self-correcting quantum many-body control using reinforcement learning with tensor networks, Nat Mach Intell **5**, 780 (2023).

[14] J. Yao, L. Lin, and M. Bukov, Reinforcement learning for many-body ground-state preparation inspired by counterdiabatic driving, Phys. Rev. X **11**, 031070 (2021).

[15] J. Nocedal and S. J. Wright, *Numerical Optimization* (Springer, New York, NY, USA, 1999).

[16] Jesper Hasseriis Mohr Jensen, F. S. Møller, J. J. Sørensen, and J. F. Sherson, Achieving fast high-fidelity optimal control of many-body quantum dynamics, Phys. Rev. A **104**, 052210 (2021).

[17] S. L. Brunton and J. N. Kutz, *Data-Driven Science and Engineering: Machine Learning, Dynamical Systems, and Control* (Cambridge University Press, Cambridge, United Kingdom, 2022).

[18] A. C. Antoulas, *Approximation of Large-Scale Dynamical Systems* (SIAM, Philadelphia, Pennsylvania, USA, 2005).

[19] Y. Kim, Y. Choi, D. Widemann, and T. Zohdi, A fast and accurate physics-informed neural network reduced order model with shallow masked autoencoder, J. Comput. Phys. **451**, 110841 (2022).

[20] I. Luchnikov, E. Kiktenko, M. Gavreev, H. Ouerdane, S. Filippov, and A. Fedorov, Probing non-Markovian quantum dynamics with data-driven analysis: Beyond "black-box" machine-learning models, Phys. Rev. Res. **4**, 043002 (2022).

[21] N. Tishby, F. C. Pereira, and W. Bialek, The information bottleneck method, arXiv:physics/0004057.

[22] N. Slonim and N. Tishby, Document clustering using word clusters via the information bottleneck method, in *Proceedings of the 23rd Annual International ACM SIGIR Conference on Research and Development in Information Retrieval* (Association for Computing Machinery, New York, NY, USA, 2000), pp. 208–215.

[23] H.-J. Liao, J.-G. Liu, L. Wang, and T. Xiang, Differentiable programming tensor networks, Phys. Rev. X **9**, 031041 (2019).

[24] J. C. Bridgeman and C. T. Chubb, Hand-waving and interpretive dance: an introductory course on tensor networks, J. Phys. A: Math. Theor. **50**, 223001 (2017).

[25] R. Orús, Tensor networks for complex quantum systems, Nat. Rev. Phys. **1**, 538 (2019).

[26] I. Oseledets and E. Tyrtyshnikov, Tt-cross approximation for multidimensional arrays, Linear Algebra Appl. **432**, 70 (2010).

[27] I. V. Oseledets, Tensor-train decomposition, SIAM J. Sci. Comput. **33**, 2295 (2011).

[28] M. Serbyn, M. Knap, S. Gopalakrishnan, Z. Papić, N. Y. Yao, C. R. Laumann, D. A. Abanin, M. D. Lukin, and E. A. Demler, Interferometric probes of many-body localization, Phys. Rev. Lett. **113**, 147204 (2014).

[29] J. Preskill, Quantum computing in the NISQ era and beyond, Quantum **2**, 79 (2018).

[30] K. Bharti, A. Cervera-Lierta, T. H. Kyaw, T. Haug, S. Alperin-Lea, A. Anand, M. Degroote, H. Heimonen, J. S. Kottmann, T. Menke, W.-K. Mok, S. Sim, L.-C. Kwek, and A. Aspuru-Guzik, Noisy intermediate-scale quantum algorithms, Rev. Mod. Phys. **94**, 015004 (2022).

[31] M. W. Doherty, N. B. Manson, P. Delaney, F. Jelezko, J. Wrachtrup, and L. C. Hollenberg, The nitrogen-vacancy colour centre in diamond, Phys. Rep. **528**, 1 (2013).

[32] H. Bernien, S. Schwartz, A. Keesling, H. Levine, A. Omran, H. Pichler, S. Choi, A. S. Zibrov, M. Endres, M. Greiner *et al.*, Probing many-body dynamics on a 51-atom quantum simulator, Nature (London) **551**, 579 (2017).

[33] J. Zhang, G. Pagano, P. W. Hess, A. Kyprianidis, P. Becker, H. Kaplan, A. V. Gorshkov, Z.-X. Gong, and C. Monroe, Observation of a many-body dynamical phase transition with a 53-qubit quantum simulator, Nature (London) **551**, 601 (2017).

[34] A. Mazurenko, C. S. Chiu, G. Ji, M. F. Parsons, M. Kanász-Nagy, R. Schmidt, F. Grusdt, E. Demler, D. Greif, and M. Greiner, A cold-atom Fermi-Hubbard antiferromagnet, Nature (London) **545**, 462 (2017).

[35] A. Bermudez, M. Martin-Delgado, and D. Porras, The localization of phonons in ion traps with controlled quantum disorder, New J. Phys. **12**, 123016 (2010).

[36] R. Barends, L. Lamata, J. Kelly, L. García-Álvarez, A. G. Fowler, A. Megrant, E. Jeffrey, T. C. White, D. Sank, J. Y. Mutus *et al.*, Digital quantum simulation of fermionic models with a superconducting circuit, Nat. Commun. **6**, 7654 (2015).

[37] U. Las Heras, L. García-Álvarez, A. Mezzacapo, E. Solano, and L. Lamata, Fermionic models with superconducting circuits, EPJ Quantum Technol. **2**, 8 (2015).

[38] M. Pasienski, D. McKay, M. White, and B. DeMarco, A disordered insulator in an optical lattice, Nat. Phys. **6**, 677 (2010).

[39] C. D'Errico, M. Moratti, E. Lucioni, L. Tanzi, B. Deissler, M. Inguscio, G. Modugno, M. B. Plenio, and F. Caruso, Quantum diffusion with disorder, noise and interaction, New J. Phys. **15**, 045007 (2013).

[40] A. Lerose, M. Sonner, and D. A. Abanin, Influence matrix approach to many-body Floquet dynamics, Phys. Rev. X **11**, 021040 (2021).

[41] A. Lerose, M. Sonner, J. Thoenniss, and D. Abanin, Influence functional of quantum many-body systems, Bull. Am. Phys. Soc. (2022).

[42] M. Sonner, A. Lerose, and D. A. Abanin, Influence functional of many-body systems: Temporal entanglement and matrix-product state representation, Ann. Phys. **435**, 168677 (2021).

[43] R. Orús, A practical introduction to tensor networks: Matrix product states and projected entangled pair states, Ann. Phys. **349**, 117 (2014).

[44] U. Schollwöck, The density-matrix renormalization group in the age of matrix product states, Ann. Phys. **326**, 96 (2011).

[45] R. P. Feynman and F. Vernon Jr., The theory of a general quantum system interacting with a linear dissipative system, Ann. Phys. **281**, 547 (2000).

[46] H.-P. Breuer and F. Petruccione, *The Theory of Open Quantum Systems* (Oxford University Press on Demand, 2002).

[47] N. Makri and D. E. Makarov, Tensor propagator for iterative quantum time evolution of reduced density matrices. I. Theory, J. Chem. Phys. **102**, 4600 (1995).

[48] N. Makri and D. E. Makarov, Tensor propagator for iterative quantum time evolution of reduced density matrices. II. Nnumerical methodology, J. Chem. Phys. **102**, 4611 (1995).

[49] A. Strathearn, P. Kirton, D. Kilda, J. Keeling, and B. W. Lovett, Efficient non-Markovian quantum dynamics using time-evolving matrix product operators, Nat. Commun. **9**, 3322 (2018).

[50] M. R. Jørgensen and F. A. Pollock, Exploiting the causal tensor network structure of quantum processes to efficiently simulate non-Markovian path integrals, Phys. Rev. Lett. **123**, 240602 (2019).

[51] E. Ye and G. K.-L. Chan, Constructing tensor network influence functionals for general quantum dynamics, J. Chem. Phys. **155**, 044104 (2021).

[52] F. Mascherpa, A. Smirne, A. D. Somoza, P. Fernández-Acebal, S. Donadi, D. Tamascelli, S. F. Huelga, and M. B. Plenio, Optimized auxiliary oscillators for the simulation of general open quantum systems, Phys. Rev. A **101**, 052108 (2020).

[53] A. Lerose, M. Sonner, and D. A. Abanin, Overcoming the entanglement barrier in quantum many-body dynamics via space-time duality, Phys. Rev. B **107**, L060305 (2023).

[54] M. Sonner, A. Lerose, and D. A. Abanin, Characterizing many-body localization via exact disorder-averaged quantum noise, Phys. Rev. B **105**, L020203 (2022).

[55] M. Suzuki, Generalized Trotter's formula and systematic approximants of exponential operators and inner derivations with applications to many-body problems, Commun. Math. Phys. **51**, 183 (1976).

[56] G. Vidal, Efficient simulation of one-dimensional quantum many-body systems, Phys. Rev. Lett. **93**, 040502 (2004).

[57] N. Boumal, *An Introduction to Optimization on Smooth Manifolds* (Cambridge University Press, 2023).

[58] P.-A. Absil, R. Mahony, and R. Sepulchre, *Optimization Algorithms on Matrix Manifolds* (Princeton University Press, Princeton, New Jersey, USA, 2009).

[59] G. Bécigneul and O.-E. Ganea, Riemannian adaptive optimization methods, arXiv:1810.00760.

[60] J. Li, L. Fuxin, and S. Todorovic, Efficient Riemannian optimization on the Stiefel manifold via the Cayley transform, arXiv:2002.01113.

[61] A. Edelman, T. A. Arias, and S. T. Smith, The geometry of algorithms with orthogonality constraints, SIAM J. Matrix Anal. Appl. **20**, 303 (1998).

[62] I. A. Luchnikov, M. E. Krechetov, and S. N. Filippov, Riemannian geometry and automatic differentiation for optimization problems of quantum physics and quantum technologies, New J. Phys. **23**, 073006 (2021).

[63] I. Luchnikov, A. Ryzhov, S. Filippov, and H. Ouerdane, Qgopt: Riemannian optimization for quantum technologies, SciPost Phys. **10**, 079 (2021).

[64] M. Hauru, M. Van Damme, and J. Haegeman, Riemannian optimization of isometric tensor networks, SciPost Phys. **10**, 040 (2021).

[65] S. Lloyd, Capacity of the noisy quantum channel, Phys. Rev. A **55**, 1613 (1997).

[66] P. W. Shor, The quantum channel capacity and coherent information, in *Lecture Notes, MSRI Workshop on Quantum Computation* (2002).

[67] I. Devetak, The private classical capacity and quantum capacity of a quantum channel, IEEE Trans. Inf. Theory **51**, 44 (2005).

[68] D. A. Abanin, E. Altman, I. Bloch, and M. Serbyn, *Colloquium*: Many-body localization, thermalization, and entanglement, Rev. Mod. Phys. **91**, 021001 (2019).

[69] P. Ponte, Z. Papić, F. Huveneers, and D. A. Abanin, Many-body localization in periodically driven systems, Phys. Rev. Lett. **114**, 140401 (2015).

[70] M. Schreiber, S. S. Hodgman, P. Bordia, H. P. Lüschen, M. H. Fischer, R. Vosk, E. Altman, U. Schneider, and I. Bloch, Observation of many-body localization of interacting fermions in a quasirandom optical lattice, Science **349**, 842 (2015).

[71] K. Slagle, Y.-Z. You, and C. Xu, Disordered XYZ spin chain simulations using the spectrum bifurcation renormalization group, Phys. Rev. B **94**, 014205 (2016).

[72] M. Serbyn, Z. Papić, and D. A. Abanin, Local conservation laws and the structure of the many-body localized states, Phys. Rev. Lett. **111**, 127201 (2013).

[73] D. A. Huse, R. Nandkishore, and V. Oganesyan, Phenomenology of fully many-body-localized systems, Phys. Rev. B **90**, 174202 (2014).

[74] M. Sonner, M. Serbyn, Z. Papić, and D. A. Abanin, Thouless energy across the many-body localization transition in Floquet systems, Phys. Rev. B **104**, L081112 (2021).

[75] M. Hauru, C. Delcamp, and S. Mizera, Renormalization of tensor networks using graph-independent local truncations, Phys. Rev. B **97**, 045111 (2018).

[76] G. Evenbly and G. Vidal, Tensor network renormalization, Phys. Rev. Lett. **115**, 180405 (2015).

[77] D. Adachi, T. Okubo, and S. Todo, Anisotropic tensor renormalization group, Phys. Rev. B **102**, 054432 (2020).

[78] K. Harada, Entanglement branching operator, Phys. Rev. B **97**, 045124 (2018).

[79] Z.-Y. Xie, J. Chen, M.-P. Qin, J. W. Zhu, L.-P. Yang, and T. Xiang, Coarse-graining renormalization by higher-order singular value decomposition, Phys. Rev. B **86**, 045139 (2012).

[80] https://github.com/LuchnikovI/Quantum-many-body-dynamics-reduced-order-modeling.